JOURNAL OF MATERIALS SCIENCE 27 (1992) 2258–2266

Transmission electron microscope study of a directionally solidified Cu–$MgCu_2$ eutectic

M. KAYA, R. W. SMITH
Department of Metallurgical Engineering, Queen's University, Kingston, Ontario, Canada K7L 3N6

The crystallography and the interface structure of a unidirectionally solidified Cu–$MgCu_2$ eutectic alloy have been examined by transmission electron microscopy. The microstructure of the eutectic was found to be lamellar and regularly interrupted by faults. The preference of the particular orientation relationship ($(\bar{1}\,\bar{1}\,1)_{Cu}//(1\,1\,\bar{1})_{MgCu_2}$) could not be explained by relative atomic densities of the planes comprising the interface. Based on the defect contrast observed and extinction distance calculations, it is suggested that the fine array of defects observed at the interface may be characterized as steps with step vectors parallel to $[1\,1\,0]_{MgCu_2}$ or $[0\,1\,\bar{1}]_{MgCu_2}$. Dislocations were also observed at the interface but they were rarely regular.

1. Introduction

Early studies of the structure of lamellar eutectics started with the observation of the preferred orientation relationship between the constituent phases. This suggested that a low-energy interface might have formed as a counter-effect to the energy gain due to the large surface area per unit volume of the interphase boundaries. Kraft [1] later suggested that the interphase boundary should consist of planes of similar density. Deviations from this hypothesis were explained by the formation of puckered planes, where the density difference between the planes on the interface was reduced by accounting for the atoms not strictly lying on that plane but close to it. In this model the predicted close-packed directions in both phases were in agreement with the observed ones.

Because eutectic alloys are produced at the eutectic melting point, after steady state growth is established, there exists a considerable chance for the defects at the interphase boundaries to arrange themselves into low-energy configurations. Transmission electron microscopy has confirmed that regularly spaced dislocation arrays exist at the eutectic interphase boundaries [2–9].

Weatherly [2] examined the interface structure in the Al–$CuAl_2$ eutectic at the fault lines. A high density of nearly parallel dislocation arrays was found. A complete determination of the Burgers vector was not possible using diffraction contrast studies.

Dislocation arrays were also reported in the interface between $CuMgAl_2$ and Al in the Al–Cu–Mg ternary eutectic [9]. Although the Burgers vectors of all the dislocations observed could not be determined, in general, some arrays gave consistent results for the Burgers vector of the $a/2[\bar{1}\,0\,1]_{Al}$ type. Because this vector does not lie in the interface it partially relieves the misfit across the interface.

Apart from misfit dislocations, ledge-type defects have also been observed in the lamellar eutectic interfaces [10–12]. Garmong and Rhodes [10–12] have observed ledges (or steps) in the Al/$CuAl_2$ and Ni_3Al/Ni_3Nb interfaces.

The present investigation was undertaken to study the crystallography and the interface structure in the Cu–$MgCu_2$ eutectic by transmission electron microscopy.

2. Experimental procedure

The Cu–$MgCu_2$ eutectic has a composition Cu–9.7 wt % Mg [13]. It was prepared from 99.99% Mg and 99.999% Cu. This alloy was prepared by induction heating in a graphite crucible under an argon atmosphere. The copper was melted first and then the magnesium was plunged into the melt by a graphite rod (see Fig. 1). The resulting liquid was then cast into 5 mm diameter rods and homogenized in graphite tubes for 2 h. The specimens were then directionally solidified at various rates between 40 and 400 mm h^{-1} using a horizontal and/or vertical Bridgman technique.

To prepare electron-transparent foils for transmission electron microscopy, an ion-beam thinning method was employed. Rods of 3 mm diameter were machined from bulk samples using electro discharge machine (EDM). In order to reduce the mechanical damage, 3 mm diameter discs of 0.5 mm thickness were cut from rods using EDM. These discs were ground down to 100 μm by a fine-grade emery paper. Final thinning was done by using an Edwards IBT 200 ion-beam thinning unit. For this, samples were thinned at an angle of 20° until perforation, then the angle was reduced to 15° and thinning continued for another 2 h. The voltage used was 4.5 kV.

The specimens were then examined in a Philips 300 and 400T electron microscopes operated at 100 and 120 kV, respectively.

 0022–2461

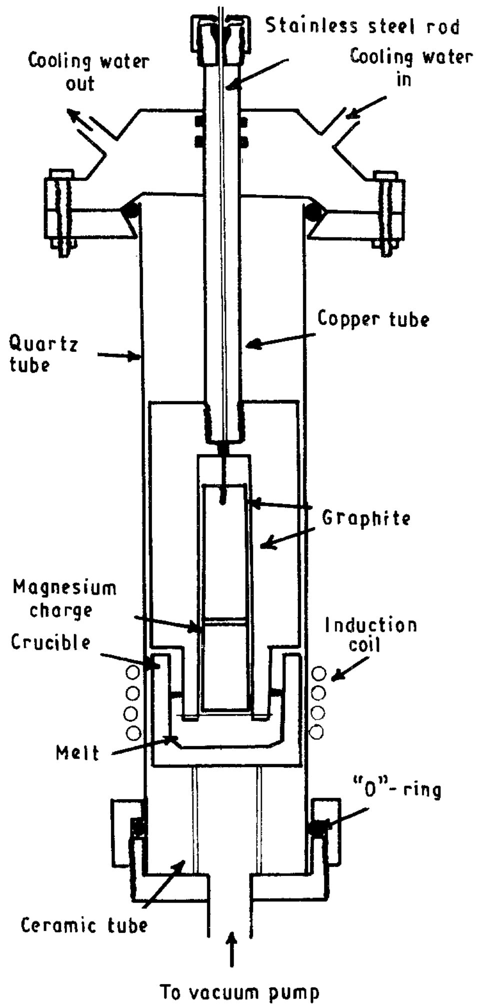

Figure 1 Plunger assembly used to produce the Cu–$MgCu_2$ eutectic melts.

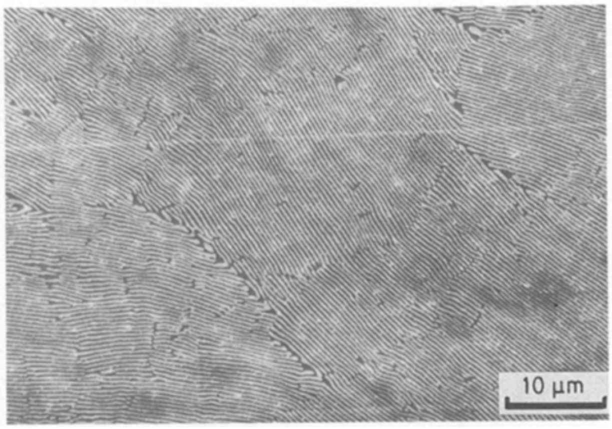

Figure 2 The microstructure of the Cu–$MgCu_2$ eutectic alloy solidified at a rate of $4 \times 10^{-4}\,m\,s^{-1}$. Transverse section.

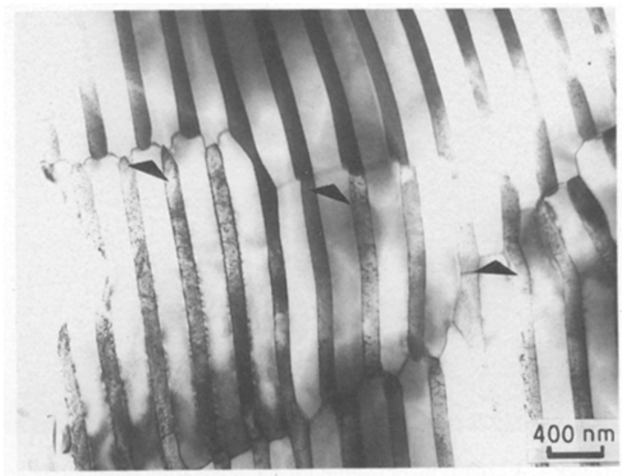

Figure 3 A transmission electron micrograph showing lamellar faults and the low-angle boundaries in the vicinity of faults in the Cu–$MgCu_2$ eutectic alloy (see arrows). Transverse section.

3. Results and discussion

3.1. Crystallography

All the samples grown by both horizontal and vertical Bridgman techniques yielded lamellar morphologies (see Fig. 2). The lamellae were regular but interrupted by faults which are characteristic of the lamellar eutectics. At certain places the eutectic lamellae had a wavy appearance. TEM analysis of the faulted areas showed that they are comprised of sub-boundaries (see Fig. 3).

The orientation relationships in the Cu–$MgCu_2$ system, as given by Fehrenbach *et al.* [14], are

$$\text{Interface plane} // (1\,1\,1)_{MgCu_2} // (1\,1\,1)_{Cu}$$

$$\text{Growth direction (to within } 7^\circ)$$

$$// [1\,1\,0]_{MgCu_2} // [1\,1\,2]_{Cu}$$

Fig. 4 shows typical micrographs from a diffraction study of the Cu–$MgCu_2$ system. Tilting the sample in a controlled way in the microscope showed that the orientation relationship is

$$\text{Interface plane} // (\bar{1}\,\bar{1}\,1)_{Cu} // (1\,1\,\bar{1})_{MgCu_2}$$

$$\text{Growth direction} // [0\,1\,1]_{Cu} // [1\,1\,2]_{MgCu_2}$$

This orientation relationship is best illustrated in Fig. 5, where it is clear that certain $\langle 0\,1\,1 \rangle$ and $\langle 1\,1\,2 \rangle$ directions are parallel. Although the samples examined showed this orientation relationship, the growth direction varied up to 10°.

The crystal structure of $MgCu_2$ is a prototype cubic Laves phase. The structure contains 24 atoms, 8 Mg and 16 Cu [15]. The atomic radii of magnesium and copper are 0.172 and 0.157 nm, respectively. It is believed that one of the main factors contributing to the existence of the Laves phases is of geometrical origin [16]. Fig. 6a shows the structure of the $MgCu_2$ phase, and the relative atomic coordinates of atoms are shown in Fig. 6b. The copper atoms are stacked as tetrahedral units, whereas the arrangement of magnesium atoms (when viewed along the $[1\,1\,1]$ direction) follows double layers of hexagonal network (see Fig. 7).

The densities of $\{1\,0\,0\}$, $\{1\,1\,0\}$, and $\{1\,1\,1\}$ planes in the $MgCu_2$ phase, calculated from the lattice parameter data [17–21], are 4.056, 11.4723 and 4.68 atom nm^{-2}, respectively. Therefore, the density of $\{1\,1\,0\}$ planes is far larger than that of other planes. The density of the $\{1\,1\,1\}$ planes in copper is 17.48 atom nm^{-2}. Hence the density misfit between $\{1\,1\,1\}$ Cu and $\{1\,0\,0\}$, $\{1\,1\,0\}$ and $\{1\,1\,1\}$ planes of $MgCu_2$ becomes 76.79%, 34.36% and 73.22%. Although the $\{1\,1\,1\}$ planes in the $MgCu_2$ structure are not the most

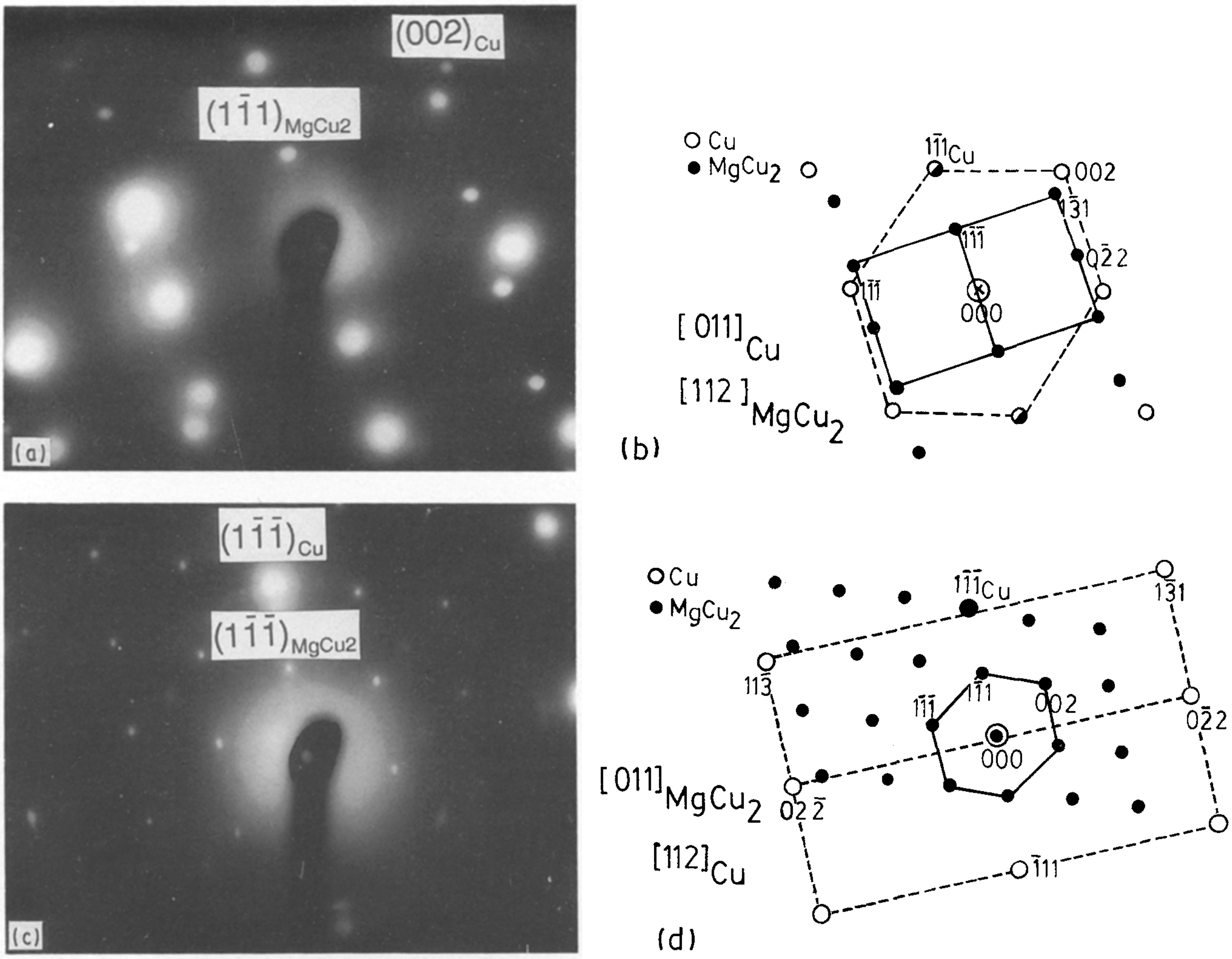

Figure 4 A typical investigation for the orientation relationship study in the Cu–$MgCu_2$ eutectic. (a) Zone axes $[0\,1\,1]_{Cu}$ and $[1\,1\,2]_{MgCu_2}$, (b) schematic drawing of (a), (c) zone axes $[1\,1\,2]_{Cu}$ and $[0\,1\,1]_{MgCu_2}$, (d) schematic drawing of (c).

closely packed planes, they still appear to form the interface.

Fig. 8a shows a $(1\,1\,0)$ projection of atoms in the $MgCu_2$ lattice. Using the structural data given by Wyckoff [15], the distances between the rows of the atoms and their coordinates after projection were calculated. It can be seen that the $MgCu_2$ structure may be constructed parallel to the $(1\,1\,1)$ plane by successive layers of magnesium and copper atoms. The stacking sequence parallel to the $(1\,1\,1)$ plane is shown in Fig. 8b. In this sequence three layers are grouped together and successive copper layers occur at regular intervals. In order to understand the details of the $(1\,\bar{1}\,1)$ plane, a perpendicular projection of the atoms lying close to this plane was made. Fig. 9 shows such a projection. It can be seen that the atoms are arranged in a hexagonal manner, where the centre of each hexagon is occupied by a copper atom. This closely resembles the hexagonal arrangement of the atoms in the $\{1\,1\,1\}$ planes of copper. It is also evident from Fig. 9 that $\langle 1\,1\,2\rangle$ directions are the close-packed directions. The density of this so-called "puckered" plane is 14.05 atoms nm^{-2}. Therefore, the density misfit between two interface planes becomes only 19.61%. If on the other hand, the next layer of copper atoms is projected on to the $(1\,\bar{1}\,1)$ plane, then the density of the plane becomes 28.1 atoms nm^{-2}. Fig. 10 shows the structure obtained with this projection. The polyhedral arrangement of the copper atoms is clearly seen.

Kraft [1], in his explanation of the preference of the $(2\,1\,\bar{1})$ plane of the $CuAl_2$ at the Al–$CuAl_2$ eutectic interface, used the "puckered plane" concept. In this analysis, several atom layers parallel to the $(2\,1\,\bar{1})$ plane were considered to behave like one plane. In order to match the density of the planes at the interface, 36% of the atoms in one of the layers were considered to contribute to this puckered plane. This was justified on the grounds that the $CuAl_2$ is considered to be deficient in copper. Therefore, for a smooth transition from $CuAl_2$ to aluminium rich solid solution, fewer copper atoms in one layer were considered to occupy the interface. Likewise, in order to match the density of the adjoining faces in Cu–$MgCu_2$, 43% of the atoms in the last copper layer must be considered to occupy the interface. However, in the Cu–$MgCu_2$ system, because the magnesium concentration from $MgCu_2$ to copper-rich solution decreases, some of the magnesium atoms in the puckered $MgCu_2$ $(1\,1\,1)$ plane should be discarded. However, the last layer in this plane is occupied only by copper atoms and the other three planes are closer to each other. Furthermore, there are not enough magnesium atoms to discard in order to match the density of

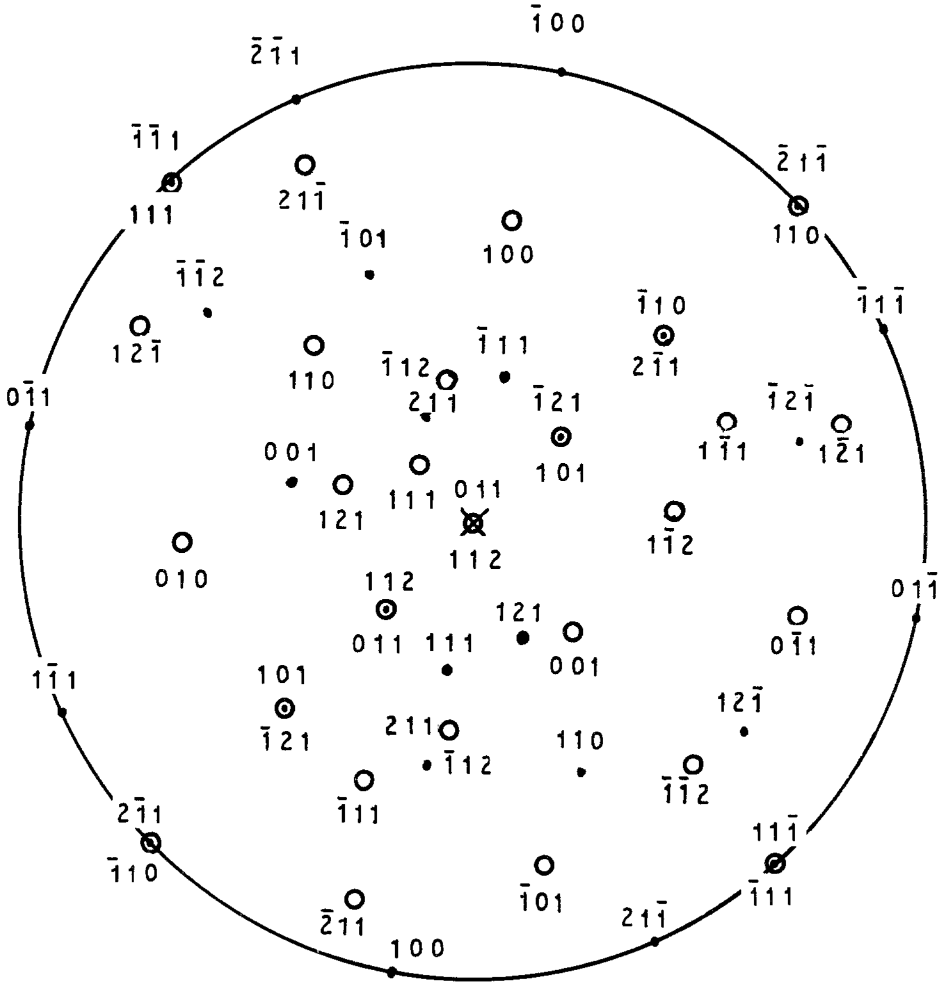

Figure 5 Superimposed stereographic projections for (0 1 1) Cu and (1 1 2) $MgCu_2$ projection normals. (○) $MgCu_2$, (●) Cu.

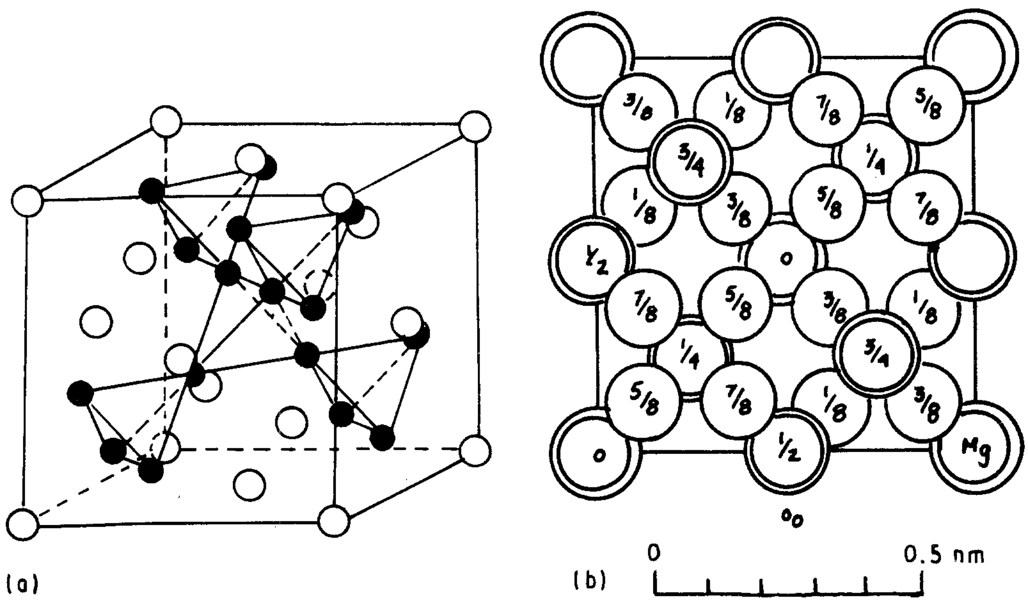

Figure 6 (a) The atomic structure of the $MgCu_2$ compound [16], (○) Mg, (●) Cu. (b) The coordinates of the atoms in the structure [15].

the planes at the interface. Therefore, density mismatch cannot be taken as the most important parameter to determine the energy of the interface in the Cu–$MgCu_2$.

3.2. Interface structure

In foils prepared from transverse sections, especially on curved portions of the lamellae, alternating black and white contrast was observed near the interface (Fig. 11). This is very similar to the contrast produced by the ledges reported by Hackney and Shiflet [16] for the ferrite/cementite interface in steels. Because, at this orientation, only a small part of the interface was visible, the remainder of the analyses were done on

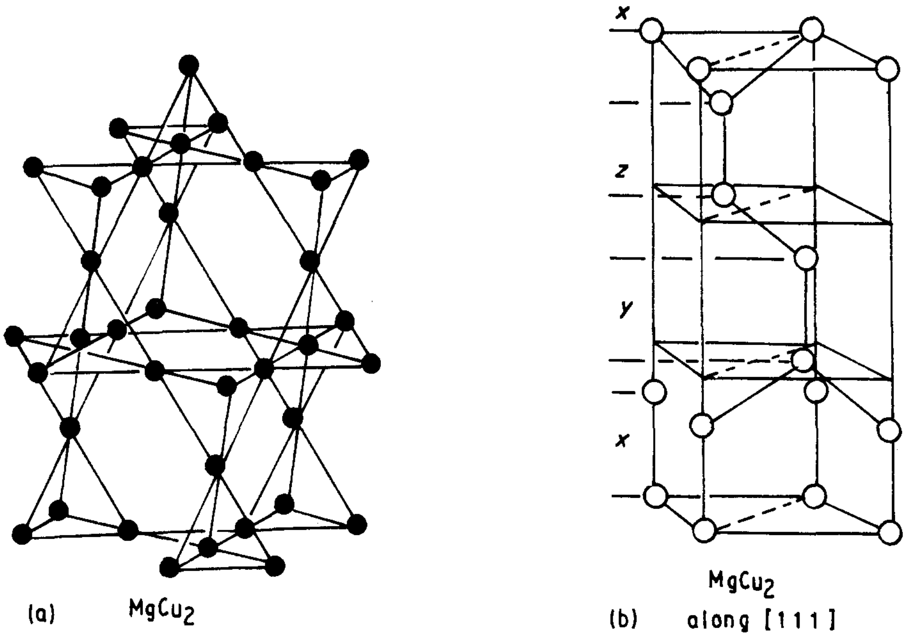

Figure 7 The tetrahedral stacking sequence of copper atoms in the $MgCu_2$ compound [16]. (b) The arrangement of magnesium atoms when viewed along the [1 1 1] direction [16].

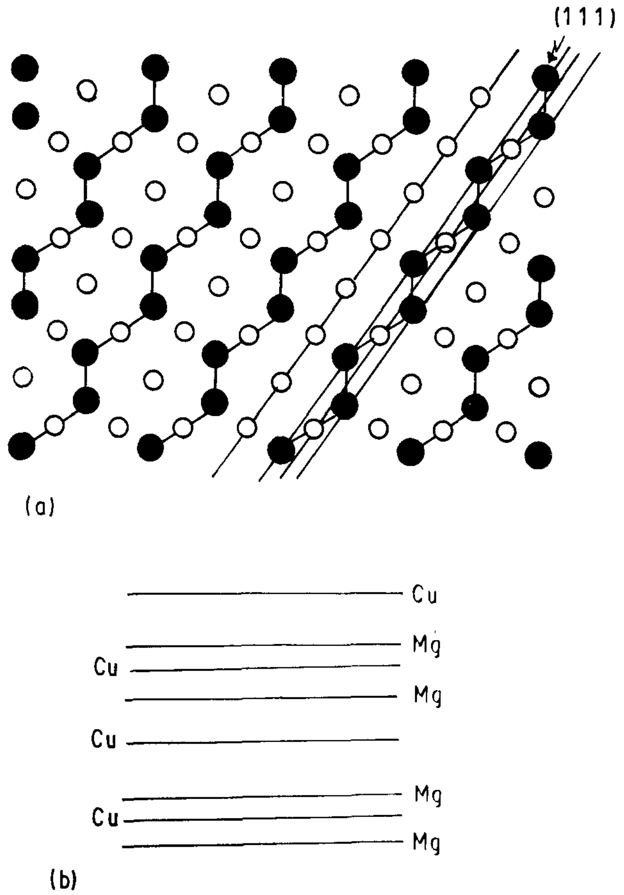

Figure 8 (a) The projection of atoms in the $MgCu_2$ structure on to the (1 1 0) plane, (●) Mg, (○) Cu; and (b) the stacking sequence parallel to (1 1 1) plane.

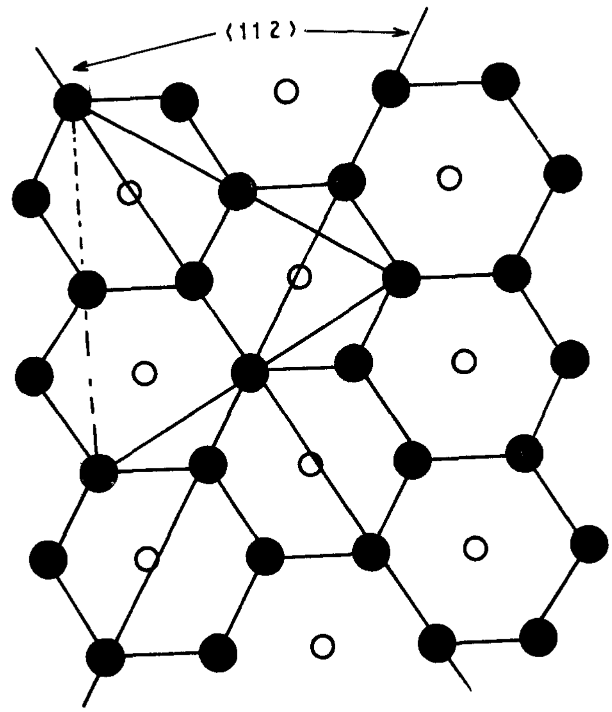

Figure 9 The projection of the atoms lying close to the (1 1 1) plane on to the (1 1 1) plane in the $MgCu_2$ structure. (●) Mg, (○) Cu.

longitudinal samples. However, at some lamellar faults, the defect structure could easily be seen (Fig. 12).

In order to identify the nature of these defects and their displacement vectors, a detailed study was undertaken using reflections from both the $MgCu_2$ and copper lattices.

The zone axes such as [1 1 0], [0 1 0], [1 2 1] and [1 1 $\bar{1}$] for $MgCu_2$ and [$\bar{1}$ 0 1], [$\bar{1}$ 1 2] and [0 0 1] for copper lattices could readily be obtained. Depending on the orientation and the limitations in the microscope, 4–6 low index reflections were obtained for each study. Fig. 13 shows several micrographs from such a study. All the micrographs were taken using $MgCu_2$ reflections in dark field. Two sets of defects are seen at the interface. Set A (as marked on the micrograph) is more regular and has a spacing of approximately 11 nm, whereas the spacing of the irregular set (Set B) varies between 20 and 60 nm.

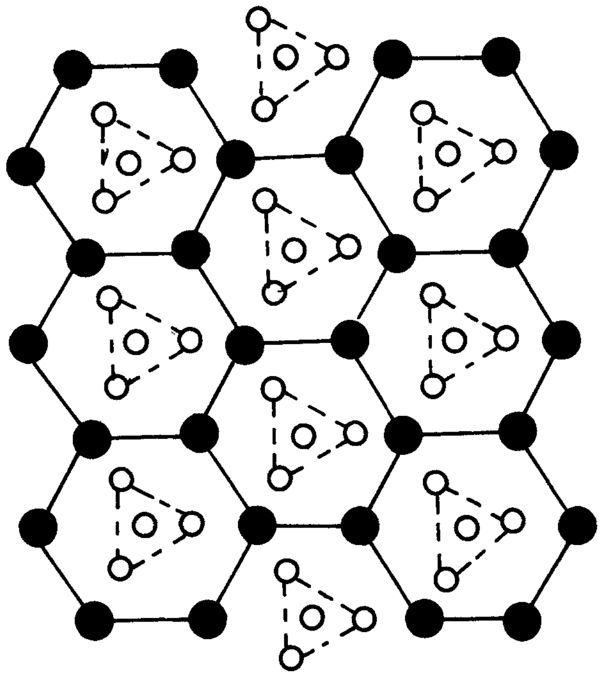

Figure 10 The projection of the atoms lying close to the (1 1 1) plane on to the (1 1 1) plane in the $MgCu_2$ structure. The next layer of copper atoms in addition to that shown in Fig. 9 is projected. (●) Mg, (○) Cu.

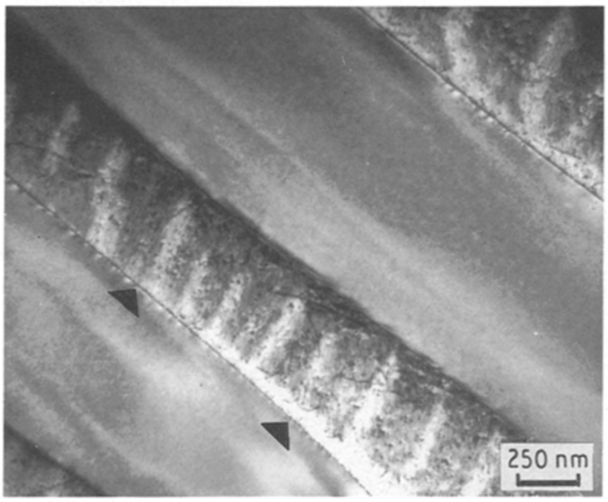

Figure 11 The defect structure of the $Cu/MgCu_2$ interface observed in the transverse section. Note the alternating black and white contrast (see the arrow).

In several areas a more regular array of defects was observed. Fig. 14 shows such an example. The spacing of the defects varies between 10 and 14 nm and 35 and 50 nm for the fine and coarse sets, respectively.

Although at least 20 interfaces were examined, it was not possible to obtain two two-beam conditions where the dislocation images were extinct, to apply the $\boldsymbol{gb} = 0$ (for screw dislocations) and $\boldsymbol{gb} \wedge u = 0$ (for edge dislocations) conditions. Since the defect width depends on extinction distances, ξ_g, these were calculated for the $MgCu_2$ lattice using the relationship [22, 23]

$$\xi_g = \frac{\pi V \cos\theta}{\lambda F_g} \quad (1)$$

where V is the volume of the unit cell, λ is the

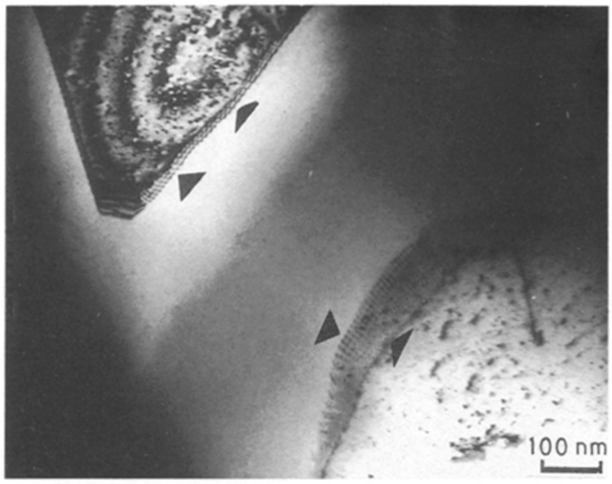

Figure 12 The defect structure found in a lamellar termination in the $MgCu_2$ structure. Note the regular single array of defects on the straight portion of the lamella while the curved section seems to contain two sets of defects.

wavelength of the electrons, θ is the scattering angle and F_g is the structure factor defined as

$$F_g = \sum_1^n f_n(\theta) \exp[2\pi i(hp_n + kg_n + lr_n)] \quad (2)$$

where h, k, l are the Miller indices of the operating reflection and f_n is the atomic scattering amplitude, and p_n, g_n, r_n are the atomic positions in the lattice. By using the atomic scattering amplitudes tabulated by Edington [22] and atomic positions by Wyckoff [15], structure factor, F_g, and then extinction distance, ξ_g, for {1 1 1}, {2 0 0} and {2 2 0} $MgCu_2$ reflections are calculated to be 144, 206 and 146 nm, respectively. This is in agreement with the finer dislocation images obtained using copper reflections such as {1 1 1}, {2 0 0} and {2 2 0}, whose extinction distances at 100 kV are 24, 28 and 42 nm, respectively.

The spacing of the fine set of defects observed using $MgCu_2$ reflections was approximately 11 nm, which corresponds to $\xi_g/13$ for {1 1 1} and {2 2 0} reflections and $\xi_g/18$ for {2 0 0} reflection. Weatherly and Mok [24] pointed out that as the dislocation spacing in the interface decreases, the volume of crystal available to produce diffraction strain contrast is reduced, thereby reducing the dislocation visibility. They calculated the minimum dislocation spacing for misfit dislocation visibility to be $\xi_g/3$ when diffraction occurred from one of the adjoining crystals and $\xi_g/6$ when both crystals are diffracting. It should be mentioned that the extinction distances will be reduced due to the many beam effects and the contribution from copper reflections which are present in certain zone axes. Even so it is unlikely that they will be reduced to values comparable to the $\xi_g/3$ and $\xi_g/6$ values predicted for the minimum spacing of the dislocations which could be resolved. Therefore, the defects observed here are probably steps and not dislocations.

Morton [25] reviewed the elastic anisotropy effects in the analysis of contrast observed from defects in TEM. In general, a dislocation in an anisotropic crystal does not leave any sets of planes flat. For cubic crystals, the anisotropy factor can be calculated from

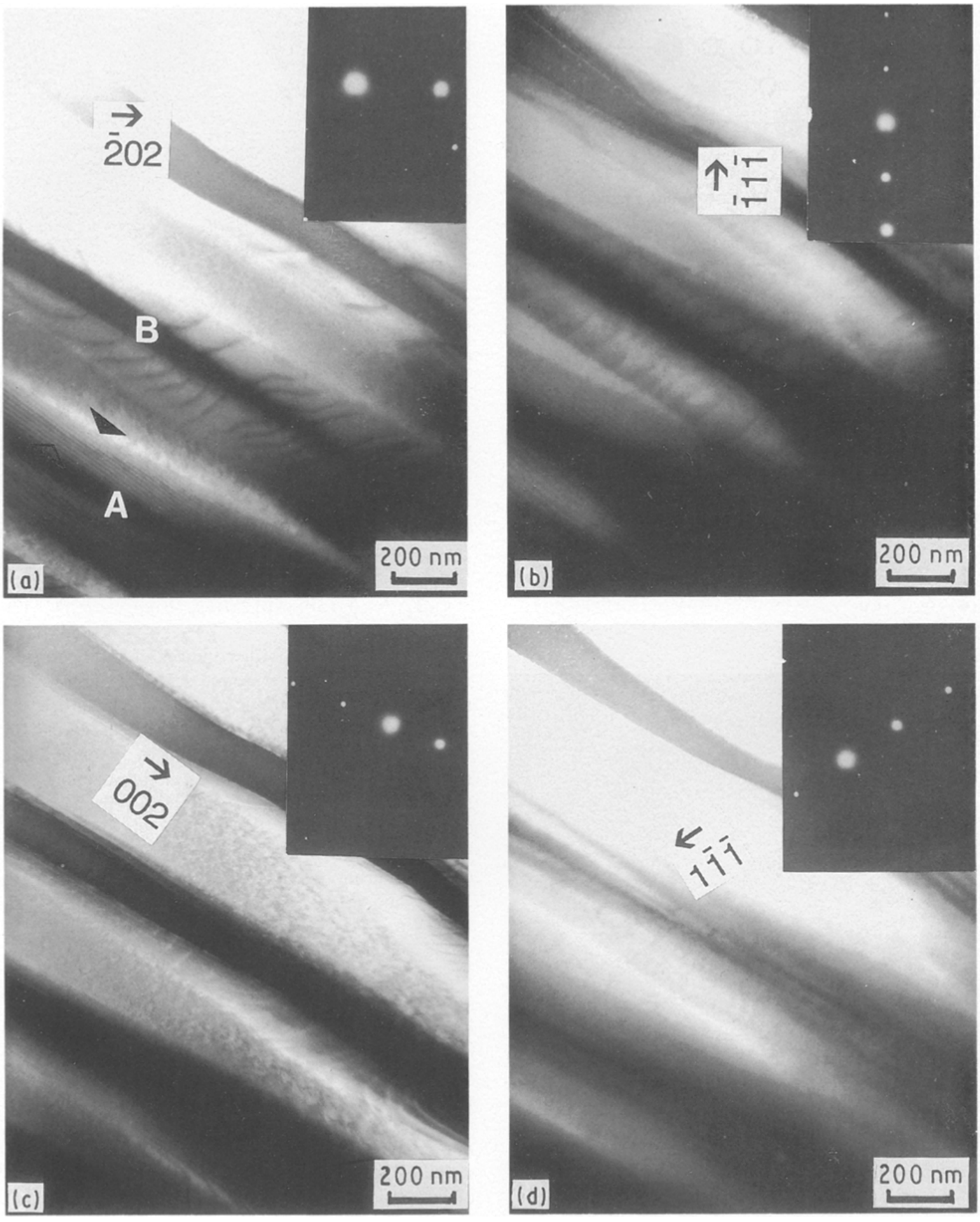

Figure 13 Dark-field study of defects in the interface using $MgCu_2$ reflections. The reflections used are: (a) ($\bar{2}$ 0 2), (b) ($\bar{1}$ 1 $\bar{1}$), (c) (0 0 2), (d) (1 $\bar{1}$ $\bar{1}$).

the elastic constants from a simple relationship

$$A = \frac{2C_{44}}{(C_{11} - C_{12})} \qquad (3)$$

where C_{11}, C_{12}, and C_{44} are the elastic constants of the cubic materials. The anisotropy factor for the copper and the $MgCu_2$ phase, calculated from the data given by Simmons and Wang [26], is $A_{cu} = 3.18$ and $A_{MgCu_2} = 1.575$. Therefore, $MgCu_2$ structure is less anisotropic than copper, which is known to be a moderately anisotropic material. Because two beam conditions were derived for elastically isotropic materials, it would apply to the $MgCu_2$ lattice better than to the copper-rich lattice. This may explain the absence of extinctions of the dislocation images using copper reflections. The only reflection which gave extinction was $(1\,\bar{1}\,\bar{1})_{MgCu_2}$. This would eliminate the possibility of displacement vectors parallel to $[1\,\bar{1}\,0]_{MgCu_2}$, $[1\,0\,\bar{1}]_{MgCu_2}$, and $[0\,1\,1]_{MgCu_2}$. The possible $\langle 1\,1\,0 \rangle$-type displacement vectors are $\pm\, a/2\,[1\,1\,0]$, $\pm\, a/2\,[1\,0\,1]$,

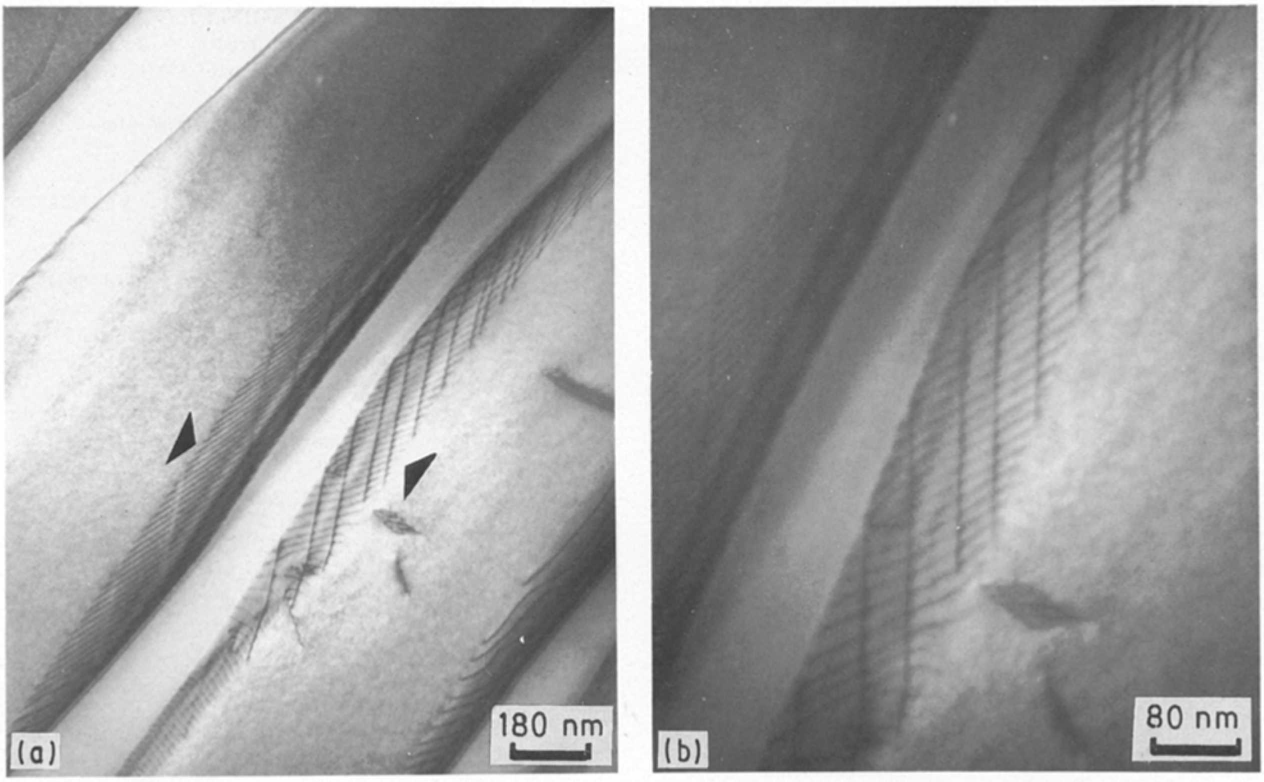

Figure 14 A regular array of defects found in a straight portion of the $Cu/MgCu_2$ interface (a), and (b) a magnified section of (a).

$\pm a/2[01\bar{1}]$. Double diffraction effects and the observed contrast at the zone axis parallel to the interface normal, made the identification difficult because two extinctions at this axis would mean a possible displacement vector normal to the interface. On the other hand, the $(\bar{2}02)_{MgCu_2}$ reflection gave consistently strong contrast, thereby eliminating the possibility of a displacement vector parallel to the $[101]_{MgCu_2}$ direction. Fig. 15 shows the hard sphere model of the interface where the (1 1 1) planes of both lattices are superimposed on each other. The misfit between the close-packed directions is 10.36%. This value is also equal to the misfit in the [1 0 1] $MgCu_2$ direction. If the misfit is fully accommodated, then dislocations every 5.4 nm with an extra plane in copper-rich lattice should occur. However, the spacing of the defects observed in this study is at least twice the size of this predicted one. Although they cannot be positively identified, the fine array of defects observed in this study are probably steps with a displacement vector parallel to $[110]_{MgCu_2}$ or $[01\bar{1}]_{MgCu_2}$. Contrary to other investigations [10–12] these displacement vectors are not normal to the interface. However, step structures with a displacement vector not lying strictly normal to the interface in an Ni–45 wt % Cr alloy, have recently been observed [27]. In this respect, these steps are similar in form to those described by Garmong and Rhodes [10–12] as Interfacial boundary dislocation-diffusion-controlled-glide (IBD–DG) ledges. Because the magnesium concentration in the copper solid solution decreases with temperature, magnesium rejection at the lamellar interface could well be established by the ledges, causing them to migrate and become bent. This process would also annihilate or agglomerate the fine ledges to form coarser ledge structures. In order to identify the nature of these defects positively, computed images are required for comparison with the observed ones.

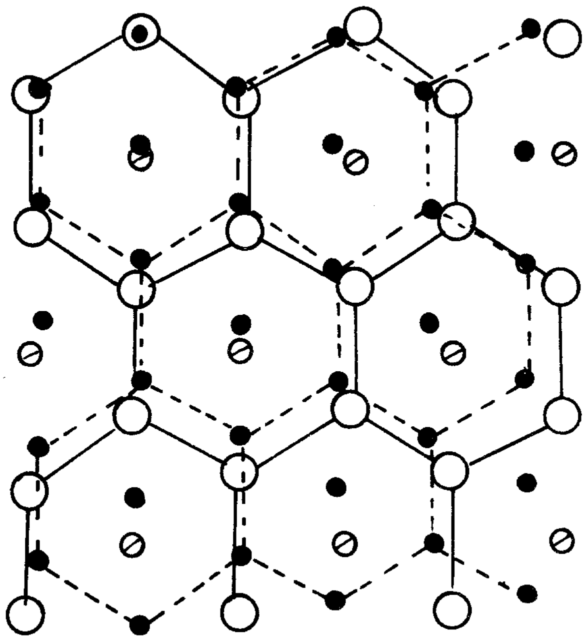

Figure 15 The hard sphere model of unrelaxed boundary structure in the Cu–$MgCu_2$ eutectic. (○) Mg, (⊘) Cu on the puckered plane, (●) Cu.

Acknowledgements
This work forms part of the eutectic research programme of R. W. Smith and has been financially supported by the National Science and Engineering Research Council of Canada and Queen's University. M. Kaya gratefully acknowledges the receipt of a McLaughlin Research Fellowship from the latter.

References

1. R. W. KRAFT, *Trans. Met. Soc. AIME* **224** (1962) 65.
2. G. C. WEATHERLY, *Metal Sci. J.* **2** (1968) 25.
3. J. L. WALTER, H. E. CLINE and E. F. KOCH, *Trans. Met. Soc. AIME* **245** (1969) 2073.
4. H. E. CLINE, J. L. WALTER, E. F. KOCH and L. M. OSIKA, *Acta Metall.* **19** (1971) 405.
5. G. GARMONG and C. G. RHODES, *Metall. Trans.* **3** (1972) 553.
6. Y. G. NAKAGAWA and G. C. WEATHERLY, *Mater. Sci. Engng* **10** (1972) 223.
7. G. D. T. SPILLER and D. A. SMITH, *J. Crystal Growth* **50** (1980) 445.
8. I. G. DAVIES and A. HELLAWELL, *Phil. Mag.* **22** (1970) 1285.
9. G. GARMONG and C. G. RHODES, *Metall. Trans.* **3** (1972) 533.
10. *Idem, ibid.* **5** (1974) 2507.
11. *Idem, Acta Metall.* **22** (1974) 1373.
12. *Idem, Metall. Trans.* **6A** (1975) 2209.
13. A. A. NAYEB-HASHEMI and J. B. CLARK, *Bull. Alloy Phase Diagrams* **5** (1984) 36.
14. P. J. FEHRENBACH, H. W. KERR and P. NIESSEN, *J. Crystal Growth* **18** (1973) 151.
15. W. G. WYCKOFF, "Crystal Structures", 2nd Edn, Vol. 1 (Interscience, New York, 1968).
16. S. A. HACKNEY and G. J. SHIFLET, in "Phase Transformations in Ferrous Alloys", edited by A. R. Marder and J. I. Goldstein (Metallurgical Society of AIME, Warrendale, PA, 1984) p. 237.
17. G. GRIME and W. MORRIS-JONES, *Phil. Mag.* **7** (1924) 1113.
18. J. B. FRIAUF, *J. Amer. Chem. Soc.* **49** (1927) 3107.
19. A. RUNQVIST, H. ARNFELT and A. WESTGREN, *Z. Anorg. Chem.* **175** (1928) 43.
20. V. G. SEDERMAN, *Phil. Mag.* **18** (1934) 343.
21. P. BAGNOUD and P. FESCHOTTE, *Z. Metallkde* **69** (1978) 114.
22. J. W. EDINGTON, "Practical Electron Microscopy in Material Science" (Macmillan, London and Basingstoke, Phillips Technical Library, 1975).
23. M. V. HEIMENDAHL, "Electron Microscopy of Materials, an Introduction" (Academic Press, New York, 1980).
24. G. C. WEATHERLY and T. D. MOK, *Surf. Sci.* **31** (1972) 355.
25. A. J. MORTON, *Metals Forum* **8** (1975) 1222.
26. G. SIMMONS and H. WANG, "Single Crystal Elastic Constants and Calculated Aggregate Properties", A Handbook, 2nd Edn (M. I. T Press, Cambridge, MA, London, UK, 1971).
27. C. P. LUO, PhD thesis, University of Toronto (1986).

Received 11 June
and accepted 1 July 1991